Proceedings of the
International Conference on Mechanical Engineering 2007
(ICME2007) 29- 31 December 2007, Dhaka, Bangladesh

ICME2007-KEY-01

Atmospheric-Pressure Plasma Microdischarges for High-Rate Deposition

Bakhtier Farouk, David Staack, Tanvir Farouk, Alexander Gutsol, Alexander Fridman
Mechanical Engineering and Mechanics
Drexel University,
Philadelphia, PA USA

ABSTRACT

Atmospheric pressure dc plasma microdischarges were generated between a thin cylindrical electrode and a flat surface. The discharge is self sustaining and of the 'cold' type − similar to the high vacuum plasma sources used in microchip manufacturing. The discharges (in argon, air, hydrogen, nitrogen and methane) were characterized both experimentally and numerically. Novel plasma reactors were constructed to investigate the discharges and use them for micro-fabrication purpose. Numerical models have been developed for hydrogen and methane/hydrogen discharges and the associated deposition processes. Plasma-assisted high-rate deposition and micro-fabrication on the substrate surface has been investigated experimentally. Gas discharges with a 'liquid-surface' electrode were also investigated experimentally.

Keywords: atmospheric pressure plasma discharge, cold plasma, microfabrication.

1. INTRODUCTION

The present study addresses the fundamental mechanisms affecting the design and operation of a novel Plasma-Assisted Net-shape Deposition (PAND) system for microfabrication. The heart of the system consists of a micron sized atmospheric pressure 'cold' plasma microdischarge which is formed between a metal-wire electrode and a substrate surface (*pin-plate configuration*). The proposed PAND method is a radically different microfabrication method, which would be an alternate to the present day photolithography or high vacuum plasma reactors. In this method, the desired 'net shape' of the film is deposited onto the substrate using plasma-assisted chemical (or physical) vapor deposition. The deposition will be carried out under atmospheric pressure and this eliminates the need for costly high vacuum reactors. The 'photo-lithography' less feature of the proposed PAND reactors will enable fabrications of sensors, small and intricate structures and devices rapidly and inexpensively. The shape and span wise dimensions of deposition can be varied by using reactors having traversing mechanism for the metal wire electrode. The traversing mechanism will enable coverage of a large surface area. The proposed plasma reactors will be developed for depositing metals, dielectric materials and polymers.

Since experimental characterization of the atmospheric pressure plasma discharge is a challenging task, the development of comprehensive process models will be critical towards obtaining time dependent physico-chemical properties of the discharge. Innovative modeling will be used to simulate the unique discharges ('cold' atmospheric pressure reactive plasma microdischarges) addressed here. High resolution 'discharge physics models' will be developed for the reactor to examine the effects of various process parameters on the plasma chemistry of the feed gases. Comprehensive numerical modeling of the process includes the consideration and interaction of the electron kinetics in the reactor; plasma chemistry of the reactive feed gases and surface reactions that affect the deposition/etching processes.

The research results can lead to the development of efficient and inexpensive microfabrication processes and reactors. Such reactors can be mass produced for ease of replacement. Significant amount of data on deposition and etching reactions under atmospheric pressure plasma conditions will be obtained. The data collected will not only be useful for developing the proposed reactors but also for further applications of the atmospheric cold plasma in other scientific areas like spectroscopy.

2. RESEARCH ACCOMPLISHMENTS

2.1 Experimental studies

From the broad perspective of using atmospheric pressure plasma enhanced chemical vapor deposition (AP-PECVD) to deposit materials the most challenging aspect is to be able to produce 'thin' films as opposed to the more common 'thick' film. The majority of technologies which produce 'thin' film operate at low pressures. This is because low pressure plasmas are well behaved since the plasma chemical-physical processes

are largely controlled by the surfaces in contact with the plasma. At atmospheric pressure the density increases and volume reactions tend to dominate over surface reactions. At these higher pressures the plasma becomes prone to overheat and is susceptible to instabilities. The major challenges of using atmospheric pressure plasmas for thin film deposition are thus: 1) creating non-thermal plasma, 2) creating stable, uniform plasmas and 3) preventing particle nucleation and growth. Our research has thus focused on 1) the fundamental characterization of microplasmas using RF and DC excitation as appropriate non-thermal plasmas and 2) deposition studies using those plasmas.

Fundamental Discharge Studies

We have created DC microplasmas in air and other gases including argon, helium, nitrogen, hydrogen, methane and some mixtures of these gases. Figure 1 is a photo of the experimental setup which is more fully described elsewhere [1]. In general a thin wire anode is suspended over a planar cathode in a discharge chamber of controllable environment. The microplasma discharge is visualized using a microscope and CCD camera. For spectroscopy a scanning monochromator with CCD detector and several tunable grating allowing for observations between 200nm and 1100 nm was used. A schematic of the circuit used to generate and analyze the glow discharge is shown in Figure 2 and is similar to that used before [1] and that used in low pressure glow discharges [2]. It consists of a DC power supply (Bertran 205B) is connected in series to a ballast resistor, and to the discharge. High frequency current and voltage probes were used to monitor the stability of the discharge.

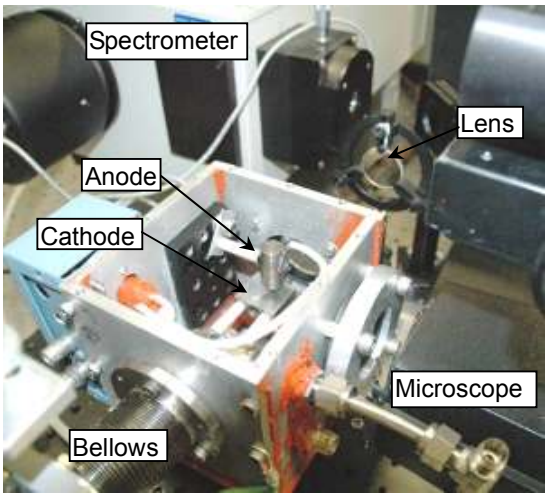

Figure 1. Photo of the experimental setup which shows the spectrometer, microscope, and discharge chamber.

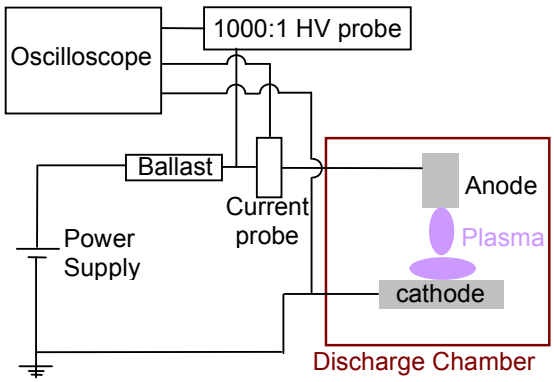

Figure 2. Schematic of the circuit for the generation of the glow discharge

Voltage-current characteristics, visualization of the discharge, estimations of current density and electric field indicate that the discharges operate in the normal glow regime. Details of these measurements were published elsewhere [1, 3]. Figure 3 shows a series of images of the glow discharge in hydrogen for increasing discharge. The anode is a wire coming from the top of the image and the cathode is the surface along the bottom edge of the image. Clearly visible in these images are the familiar bright and dark regions of a low pressure glow discharge. Beginning near the cathode we see the 'negative glow' region which increases in diameter with current such that the current density is constant. Moving up from the 'negative glow' we have the 'Faraday dark space' followed by the 'positive column'. Within the positive column striations are visible. Plots of the voltage as a function of current for the glow discharges, operated in various gases, are shown in Figure 4. These general visualizations of our glow discharge along with measured flat voltage current characteristics and constant current density in the negative glow of the discharge classify it as a density scaled version of the normal glow discharge well known from low pressure plasma discharge studies.

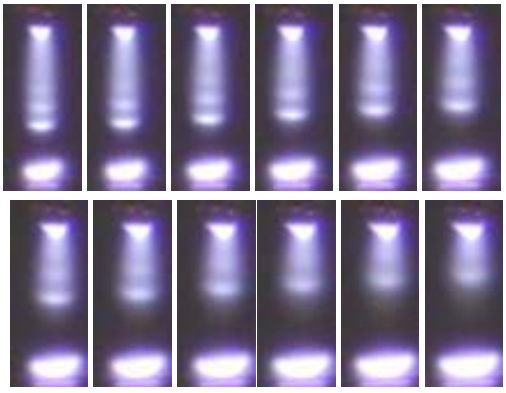

Figure 3. Striated discharges in hydrogen for 400 µm electrode spacing 1.1mA to 1.6 mA (top row) and 1.7 mA to 2.2 mA (bottom row) at 0.1 mA increments.

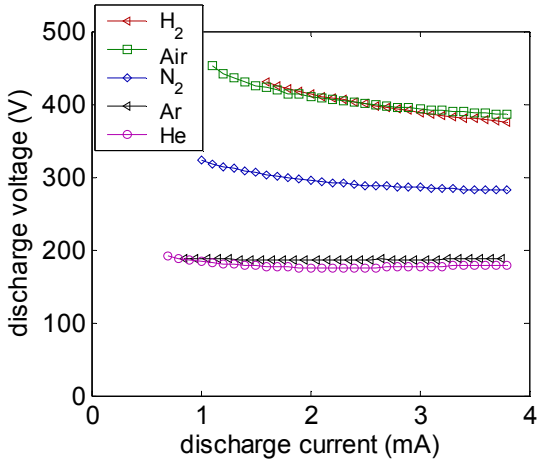

Figure 4. Voltage vs. Current for DC glows in hydrogen, air, nitrogen, argon and helium at 400 μm electrode spacing.

Figure 5 shows the results of the optical emission spectroscopy gas temperature measurement. These were attained by adding trace amounts of nitrogen to the gas and comparing measured and modeled spectra from the N_2 2nd positive system.[4] In general atomic gases are cooler than molecular gases and gases with higher thermal conductivity are cooler as well. Since the temperature is a balance between electron impact induced heating and diffusive cooling these indicate that the atomic gases are less heated by the electrons. This is due to the molecular gases having addition paths of energy transfer from the electron temperature to the gas temperature; namely electron-vibrational (e-V) modes and vibrational-translational (V-T) modes which results in more energy transfer to the gas. [5]

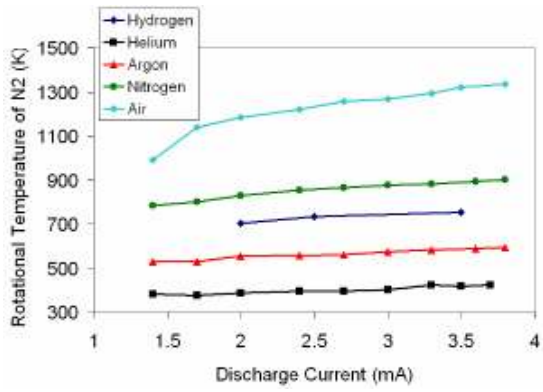

Figure 5. Gas temperature measurement using addition of trace N_2 in normal glow at 0.3 mm electrode spacing for hydrogen, helium, argon, nitrogen, and air.

Materials Deposition Studies

Preliminary PECVD studies using methane as a precursor in hydrogen led to the deposition of amorphous carbon deposition of various types (diamond-like hydrogenated carbon, graphite-like hydrogenated carbon, polymer-like hydrogenated carbon). These were identified through Raman spectroscopy and FTIR vibrational spectroscopy. However, the overall deposition quality was poor due to the deposition of films with very high surface roughness. Microscope visualization and profilometry of the surfaces revealed it to be made up of an agglomeration of micron sized particles.

The source of this surface roughness was identified to be due to 1) instabilities in the plasma discharge and 2) particle formation in the volume of the discharge which then deposits onto the surface. The instability consisted of transition of the normal glow discharge into a very high current discharge and then extinguishing of the plasma and re-ignition with repetition frequencies on the order of 100s kHz for DC plasmas. The instability causing this effect was identified as the ionization overheating instability. [6]

This instability is indicated in the close chain shown below schematically. An incremental increase in the electron density (n_e) leads through collision to an increase in gas temperature (T_o=T_{trans}). The T_o increase corresponds with a decrease in neutral density, n_o, by the equation of state at constant pressure. The decrease in density corresponds to an increase in the parameter *E/n* assuming a constant electric field, *E*. The electron temperature (T_e) is largely determined by *E/n* and an increase in *E/n* causes and increase in T_e. At slightly higher T_e the ionization rate increases dramatically and causes a further increase in n_e. The chain thus has positive feedback and is unstable. This mechanism is one of the major mechanism by which a non-thermal discharge becomes a thermal discharge.

$$\uparrow n_e \Rightarrow \uparrow T_o \Rightarrow \downarrow n_o \Rightarrow \uparrow \frac{E}{n} \Rightarrow T_e \Rightarrow \uparrow n_e$$

Figure 6. Schematic representation of the instabilities in the plasma discharge

In low pressure plasmas this instability is suppressed by cooling of the plasmas discharge on the chamber walls. At atmospheric pressure the electrode surfaces cannot provide sufficient cooling even at the reduced sizes in a microplasma [7]. A von Neumann perturbation analysis and analytical modeling of the discharge confirmed the effect of the external circuit. An approximate formula for the growth rate of the instability, Ω, derived from the instability analysis is shown in equation 1, where k_i is the ionization rate, T is the gas temperature, ν_h is the gas heating frequency, ν_c is the gas cooling time, V is the discharge voltage, and ν_d is the external circuit response frequency (1/RC). From these equations we see that for the DC plasmas a new method of suppressing these instabilities by minimizing the stray capacitance in the external circuit. In such a situation the increase in n_e will be accompanied by a decrease in E through the external circuit such that there is no net increase in E/n and the instability is suppressed.

$$\Omega \approx \frac{d\ln k_i}{d\ln T}\nu_h - \nu_c - \frac{d\ln k_i}{d\ln V}\nu_D \qquad (1)$$

These effects were seen in the visual characteristics of the discharge and time resolved current measurements.

Figure 7 shows a comparison of the unstable and stabilized glow discharge in Hydrogen. Only in the stabilized glow discharge are the striations visible and the negative glow has a normal current density. Also current and voltage measurements of the unstable glow show that although the applied voltage is DC there is a oscillation in the external circuit driven by the ionization overheating instability and parasitic capacitance which causes the discharge to rapidly increase in current and then shut off at frequencies on the order of 100 kHz.

Figure 7. Image of stabilized and self pulsating glow discharges in hydrogen.

The fundamental studies of the energy transfer within the plasma discussed earlier and the new method to stabilize the plasma discharges is important in seeking to perform plasma enhanced chemical vapor deposition (PECVD). In such complex chemical systems the precursor gases are typically molecular with many vibrational modes. As such the energy transfer from the electrons to the gas can be significant leading to both increased temperatures and instabilities. Through these studies we have found that these problems can be ameliorated by 1) modifying the external circuit to stabilize the discharges and 2) using high thermal conductivity buffer gases to lower the gas operating temperature. By suppressing the instabilities films with regions of uniform smooth features could be attained. However, particles from 100's nm to 10's um in size could be uniformly distributed within this 'thin' film, as shown in Figure 8a. Particle, or soot, nucleation for plasmas with CH_4 precursors is known to be highly temperature dependant and due to the formation of C_2H_2. Experimentally by varying the discharge power, methane fraction, and gas temperature (through Helium buffer addition) regimes of particle free thin film deposition were found, as shown in Figure 8b. As expected these regimes were found at lower methane concentration, lower discharge power, and lower gas temperature.

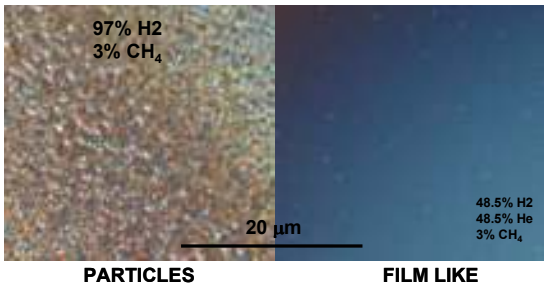

(a) (b)

Figure 8. Images of deposited film from (a) particle-regime and (b) film-regime of the PECVD.

Exploratory studies of gas discharges with a liquid surface electrode

Gas-phase atmospheric pressure discharges produced using one or more liquid electrodes have been studied recently for their potential application in water treatment, micro and nano-machining and surface deposition [8-12]. However, the majority of the studies have focused on discharges sustained at relatively large currents (at several 10s of milliamperes). Until recently, discharges produced at significantly lower currents—namely, at currents on the order of several milliamperes—have remained largely unexplored.

Experiments were conducted to identify the properties and behavior of a dc, atmospheric pressure glow discharge produced using one metal electrode and one electrolytic liquid electrode, at currents on the order of 1 mA. Deionized water and tap water is used as the electrolytic electrode for the studies. Interestingly, it is also found that, at certain points in this current regime, discharges initiated exhibit a unique "spinning" behavior, in which the end nearest the liquid electrode spins, while the end near the metal electrode remains stationary. While behavior similar to this has been noted before [13], a study focused on the characteristics and causes of such behavior has not been performed before.

The general reactor setup used to produce the discharges studied in these experiments is pictured in Figure 9. Here, a steel, approximately hemispherical electrode of ~5 mm in diameter is suspended by an x-, y-, and z-positioner over a large steel tub filled with water solution. The tub is fixed to a stand which may also be moved in the x-, y-, and z-directions. Using a large tub ensures that the water level will not change significantly due to evaporation that occurs during discharge operation, and thus that the electrode gap length changes by only a small amount during prolonged discharge operation (in an hour of continuous discharge operation at moderate currents, the water level was found to drop by approximately 0.1 mm; thus, deviations in the discharge lengths discussed in this paper are considered to be approximately ±0.1 mm). For the majority of the experiment, discharges in AP air were studied, and in this case, the electrode configuration was left open in the ambient environment.

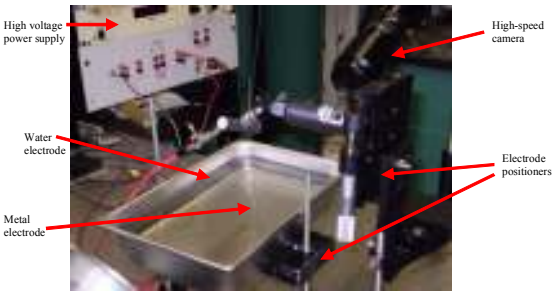

Figure 9. Photograph of the general discharge reactor setup, along with some of the analytic equipment used in these experiments.

Figure 10. An image of the spinning discharge produced with deionized water as the anode at an electrode gap of 7.5 mm, captured with an exposure time of 1/60 s.

Figure 10 presents an image of the discharge in the spinning regime at a gap length of 7.5 mm, taken with an exposure time of 1/60 sec. At this exposure time, the discharge appears to take on a bell-like shape. However, Figure 11 shows a series of photos of the same discharge at a smaller exposure time of 1/160 sec; from these photos, a single discharge with the same structure as the stationary discharge becomes distinguishable, for which the cathode spot remains in a relatively fixed position over time, while the anode spot moves in a closed loop. This suggests that the discharge visible in this regime of motion is indeed a spinning version of the stationary discharge produced.

Figure 11. A sequence of images of the spinning discharge with deionized water as the anode at an electrode gap of 7.5 mm, each captured at an exposure time of 1/160 s.

In the set of images above, the negative glow (NG), Faraday dark space (FDS), positive column (PC), low-luminosity region of the positive column (LL), and anode glow (AG) are all clearly visible, and it becomes evident that the anode spot of the discharge in the spinning regime is in fact rotating while the negative glow remains stationary.

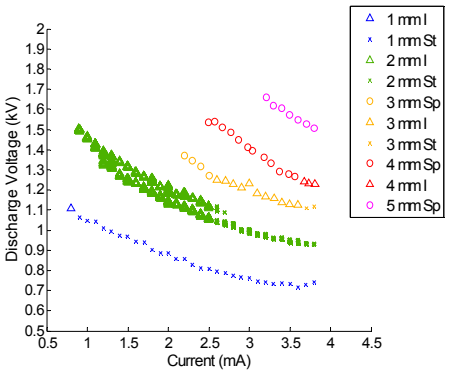

Figure 12. Voltage-current measurements for an AP air discharge produced with a steel, hemispherical, 5-mm diameter cathode and a tap water anode at various gap lengths. Here, "St" denotes a discharge in the stationary regime, "I" denotes a discharge in the intermediate regime, and "Sp" denotes a discharge in the spinning regime. Deviations in voltage measurements were calculated and did not exceed 40.0 V.

In general, the voltage-current curves shown in Figure 12 are very similar in terms of behavior to those representative of a normal glow discharge operating between two metal electrodes [14]. Here, for a fixed gap length, the discharge voltage decreases only slightly with increasing discharge current, and the discharge voltage required to operate a discharge at a fixed current increases with increasing gap length. For a normal glow discharge, the voltage typically remains relatively constant with increasing current for a fixed length, and the discharge voltage increases for a fixed discharge current with increasing electrode gap length, as well. The slight trend of decrease may be explained by small increases in discharge temperature with increasing current, which, at constant pressure, would decrease the density and thus the resistance of the discharge region. This difference aside, though, the high degree of similarity between the voltage-current measurements of the discharge studied here and that of a normal glow discharge over all regimes of motion further suggests that the discharge being studied is a normal glow, both in the stationary and spinning stages.

2.2 Computational and modeling studies

Modeling of the present 'cold' atmospheric pressure plasma microdischarge poses unique challenges. While the atmospheric pressure condition means high densities for all species, the micron scale discharge reduces the size of the computational domain. A multi-dimensional hybrid model has been developed in the present study to characterize the glow discharge operating at atmospheric pressure. In conventional fluid models, the reaction rates are expressed in Arrhenius form, assuming a Maxwellian electron energy distribution function (EEDF). To account for the non-equilibrium nature of the microdischarge at

atmospheric pressure in the hybrid models, a Boltzmann solver for calculation of the EEDF is implemented. The electron transport parameters (mobility, diffusion coefficients), electron temperature and electron induced reaction rates are obtained by solving the two-term spherical harmonic expansion of the Boltzmann equation [15]. Using this model, two-dimensional simulations are performed for hydrogen discharge in a 'pin-plate electrode configuration' driven by a DC power source connected through a simple resistive-capacitive circuit. One dimensional simulation for a DC methane-hydrogen discharge with a *plate-plate* electrode configuration was also conducted to predict diamond like carbon (DLC) deposition. Simulations are carried out for different values of ballast resistance.

The mathematical model employed is similar to that used in our previous studies [16]. The discharge model consists of coupled conservation equation for the different species (electrons, ions, excited species and neutrals) conservation of the momentum and energy for the multi-component fluid mixture, state relations and the Poisson's equation. A conservation equation for the electron energy T_e is not modeled and solved. Instead, the local-field approximation appears to be more appropriate for the present atmospheric pressure plasma discharge being considered. Based on the local-field approximation the electron transport properties (mobility μ_e and diffusivity D_e) and electron energy T_e and electron induced reaction rates are considered to be a function of the local electron density (n_e) and the reduced electric field (*E/N*). The values are computed by using a lookup table constructed by solving the zero-dimensional Boltzmann equation over a range of n_e and *E/N* [17]. The look-up tables are prepared first and used for the present plasma calculations instead of running the numerically expensive Boltzmann solver simultaneously with the discharge simulation model.

Figure 13 depicts the computational domain for the simulation of atmospheric pressure micro discharge in hydrogen for a *pin plate electrode configuration* (metal wire tip and a planar metal surface). The inter-electrode separation is set to 400 μm. A cathode radius of 500 μm was chosen so that zero-gradient boundary conditions could be applied along the boundary c-d-e. The electrodes are coupled to an external circuit. The external circuit contains a resistance *R* and a capacitance *C* connected in series and in parallel respectively (Figure 14). The ballast resistance *R* is required in order to limit the discharge current, preventing the discharge from

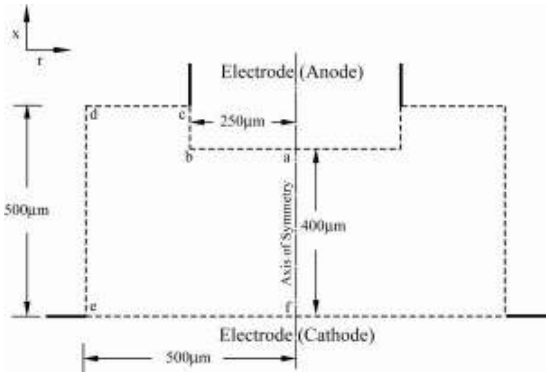

Figure 13. Schematic diagram of the computational domain (enclosed in dotted line).

reaching an abnormal (high current) mode. The capacitance *C* represents the parasitic capacitance which is present in the experiments intrinsically due to the external cables. The parasitic capacitance *C* introduces a time delay between the applied voltage V_{pwr}, and the discharge voltage, V_d. When enough voltage is applied between the cathode and the anode, the plasma is self sustained by secondary electrons emitted from the cathode due to ion impact. In these simulations the supply voltage V_{pwr}, is fixed at 1200 V, because for a 400 μm inter-electrode separation, the breakdown voltage is 1200 V for hydrogen gas at atmospheric pressure [5]. The ballast resistance is varied from 800 kΩ to 150 kΩ and the capacitance *C*, is fixed at 0.1 pF, which corresponds to the estimated value for the experimental setup.

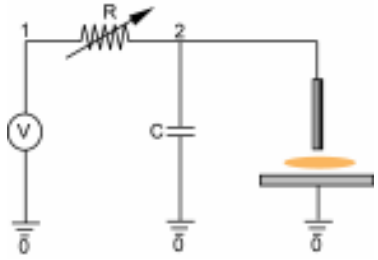

Figure 14. Resistive capacitive circuit for the plasma discharge '0' indicates grounded nodes. The voltage supply is between nodes '0' and '1'.

The hybrid model was developed for hydrogen gas. The species considered include H, H_2, H^+, H_2^+, H_3^+, $H^*(2p)$ H_2^* ($C^1\Pi_u$ 2pπ), $H_{2\ v=1}$ and the electrons. The dominant reactions were identified under the operating conditions of the micro-discharge. The reactions were also selected so that all species had source and sink terms to bound the production rate. The reactions can be grouped into seven categories 1) elastic collisions 2) dissociation 3) ionization 4) electron-ion collisions 5) ion-neutral collisions 6) neutral-neutral collisions and 7) excitation and de-excitation [18, 19]. Since for a diatomic molecule most of the electron energy goes into the vibrational excitation [5] it is crucial to include

vibrationally excited species in the chemical reaction scheme in order to obtain an accurate EEDF. In the model only the first levels of the electronic and vibrational excitations (v = *1*) are taken into account. This simplification is done in order to reduce the computational time. The simplification is justified because these are the most populous excited species due to their lowest excitation energies.

In this work, the CFD-ACE+ code [20] is used to simulate the plasma and a general purpose circuit simulator, SPICE [21] is used to simulate the external circuit. The CFD-ACE+ solver calculates the transport of the charged and neutral particles and electric field by solving the PDE's. The solver calculates the currents at the electrodes for a given potential at the electrodes. Based on the currents the SPICE code recalculates the voltage at the electrodes by solving the ODE's for the external circuit. For each time step, the overall solution is iterated until the convergence of voltage/current is reached.

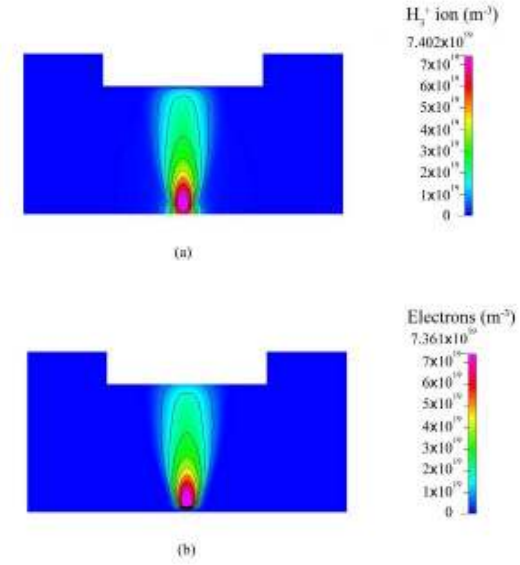

Figure 15. Contour plot of constant a) H_3^+ ion density (maximum value 7.40 x 10^{19} m^{-3}) and b) electron number density (maximum value 7.36 x 10^{19} m^{-3}). Ballast resistance 400 kΩ, V_d = 375 V and I_d = 2.06 mA [22].

Contour plots of constant H_3^+ ion and electron density are shown in Figures 15 (a) and (b). For this simulation the external circuit had a ballast resistance of 400 kΩ. From the contour plots of H_3^+ and electron density it can be seen that both the H_3^+ ions and electrons have the maximum density near the cathode region. This indicates that there exists a significant volumetric production of these species near the cathode of the discharge. The high electric field at the cathode is responsible for the large volumetric production of electrons and H_3^+ ions near the cathode. The production of electrons is well balanced by the production of H_3^+ ions resulting from the ion-neutral collisions of H^+ and H_2^+ ions with hydrogen molecules and also the collisions of electronically excited atomic hydrogen with hydrogen molecules. Peaks in electrons and H_3^+ ion concentration corresponds to the negative glow of the discharge.

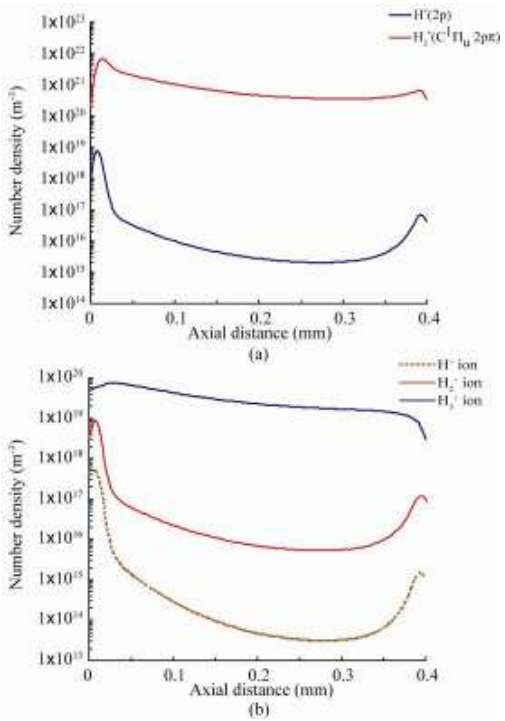

Figure 16. Species density along the axial distance(r = 0) a) Electronically excited species ($H^*(2p)$ and $H_2^*(C^1\Pi_u$ 2pπ)) b) Ionic species (H^+, H_2^+ and H_3^+). Ballast resistance 400 kΩ, V_d = 375 V and I_d = 2.06 mA [22].

Figure 16 summarizes the different species (ions, electronically excited states) density distribution along the axial distance. The predicted H_2^* ($C^1\Pi_u$ 2pπ) is found to be three orders of magnitude higher than that of H^* (2p). The axial distribution of the electronically excited hydrogen species indicates higher density of H_2^* ($C^1\Pi_u$ 2pπ) and H^* (2p) near the electrodes, with larger density near the cathode. The electronically excited species density drop near the electrodes owing to the surface quenching effect resulting from the surface reactions. It is known that the electronically excited species ($H^*(2p)$ and H_2^* ($C^1\Pi_u$ 2pπ)) is responsible for the brightness of the glow discharge. The electronically excited species distribution indicates two luminous zones, existing near the electrodes. Contour plot of the combined electronically excited species ($H_2^*(C^1\Pi_u$ 2pπ) + $H^*(2p)$) (Figure 17) clearly shows the two bright zones in the discharge. The luminous regime near the cathode and the anode denotes the 'negative glow' and the 'anode glow' respectively. The 'negative glow' is found to be much larger than the 'anode glow'. Distribution of the ionic species (H^+, H_2^+ and H_3^+) along the axial distance (figure 13 (b)) shows the heavier H_3^+ ion to be the dominant ionic species. The calculations predicted the heavier H_3^+ ion to be one order of magnitude higher than H_2^+ and two orders of magnitude higher than H^+ ions. As seen for the electronically excited species the ionic species also showed a similar peak density near the cathode. Peaks in the ion concentrations correspond with the negative glow of the discharge.

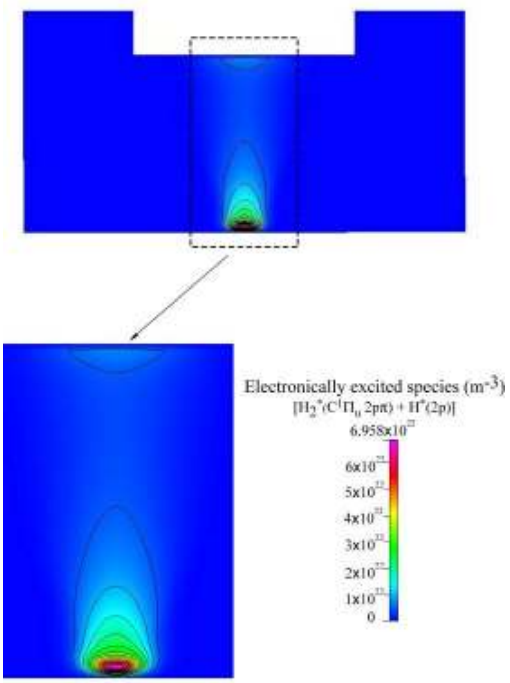

Figure 17. Contour plot of constant electronically excited species ($H_2^*(C^1\Pi_u\ 2p\pi)$ + $H^*(2p)$) density (maximum value 6. 95 x 10^{19} m^{-3}). Ballast resistance 400 kΩ, V_d = 375 V and I_d = 2.06 mA [22].

Figure 18 shows the temperature profile along the axial distance for various discharge currents. Significant gas temperatures are observed due to ion Joule heating and the Frank Condon effect. For all the cases the gas temperature peaks at the cathode sheath where the electric field is the maximum. Positive ions gain energy from the electric field and collisionally transfer this energy to the neutral gas, thereby heating the gas. The gas heating outside the sheath was a result of the Frank Condon heating.

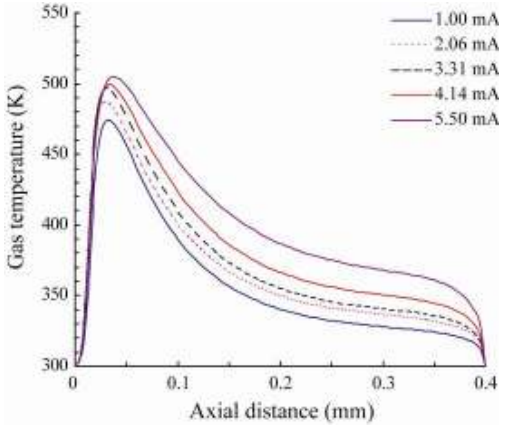

Figure 18. Calculated gas temperature along the axial distance of the discharge (r = 0) for different discharge current (1.00, 2.06, 3.31, 4.14 and 5.50 mA) [22].

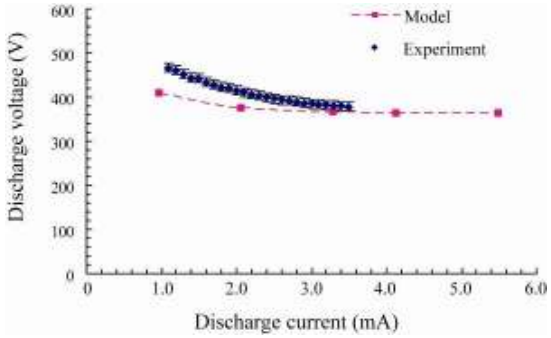

Figure 19. Voltage-current characteristics of the atmospheric pressure hydrogen micro-discharge [22].

The resulting voltage-current (V-I) characteristics from the simulations is shown in Figure 19. The flat nature of the V-I curve signifies the existence of the normal glow-discharge regime [5]. In the normal glow discharge the voltage remains constant, with increasing current resulting due to the formation of the "normal current density". From the V-I characteristics it can be seen that the normal glow regime initiates for a discharge current greater than 1.0 mA. Model predictions agree well with the experimental data. The obtained V-I characteristics is similar to those observed for a low pressure DC discharge [2].

The physical and chemical properties of diamond-like carbon (DLC) layers make it an ideal candidate for applications such as machine tools, optical coatings and high temperature electronics [23]. Plasma discharges have been used frequently for the deposition of these DLC layers by utilizing plasma-assisted chemical vapor deposition (PACVD) process [24-26]. These processes in general utilize CH_4 as the carbon bearing feedstock and dilute it with large amounts of H_2 to obtain these DLC layers. Furthermore all these plasma sources are generally maintained at low pressure for the deposition process. Atmospheric pressure glow discharges are attractive for a wide range of material processing application largely due to their operation flexibility afforded by the removal of the vacuum system. Experimental studies are being performed to use the atmospheric pressure micro normal glow discharge [3] for DLC deposition. In order to improve the deposition process, a DC powered methane – hydrogen discharge has been simulated to obtain insight into the physico-chemical processes. This would enable the optimization of the plasma parameters (power, gas mixture, gas flow) for good quality deposition.

The model employed was similar to that of the atmospheric pressure DC hydrogen discharge [22]. The only difference was the increased number of species that were considered for a methane-hydrogen discharge. The species considered include 8 neutral species (C, CH_4, C_2H_2, C_2H_4, C_2H_6, C_3H_8, soot and H_2), 8 ionic species (CH_3^+, CH_4^+, CH_5^+, $C_2H_2^+$, $C_2H_4^+$, $C_2H_5^+$, H_2^+ and H_3^+), 7 radicals (CH, CH_2, CH_3, C_2H, C_2H_3, C_2H_5 and H) and the electron. These species were identified from the dominant reaction chemistry of methane-hydrogen plasma in atmospheric pressure and the reaction rates

were obtained from the literature [27, 28] . Since one of the major objectives was to predict DLC deposition phenomena, the surface chemistry model included 17 surface species (physi-sorpted and bulk). It consisted of 81 reactions describing physisorption, chemisorption, desorption, sputtering, stitching, surface ion-electron recombination, radical-surface and molecule-surface reactions. To predict the quality of the deposited film the surface-chemistry model had diamond-like carbon, graphitic carbon and soot as the bulk deposited species.

Simulations were carried out for atmospheric pressure methane-hydrogen discharges for five cases of varying ballast resistance (200 kΩ, 400 kΩ, 600 kΩ, 800 kΩ and 1000 kΩ). For all the cases the gas mixture had 99% H_2 and 1% CH_4. Figures 20 and 21 show the distributions of the different ionic species along the axial distance. It can be seen that the H_3^+ is the dominant hydrogen ion and it has the maximum value of 6 x 10^{19} m^{-3} in the volume of the discharge. The H_2^+ ion was found to be one order of magnitude smaller than the H_3^+ ions. The H_2^+ ions had the maximum value at the cathode sheath and a lesser peak in the anode sheath. This indicated that the H_2^+ ions were being formed in the sheath regions of the discharge.

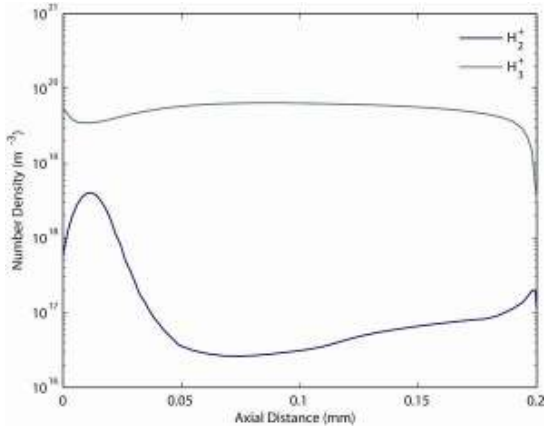

Figure 20. Hydrogen ionic species density along the axial distance (ballast resistance 200 kΩ, V_d = 251.1 V, I_d = 4.74 mA).

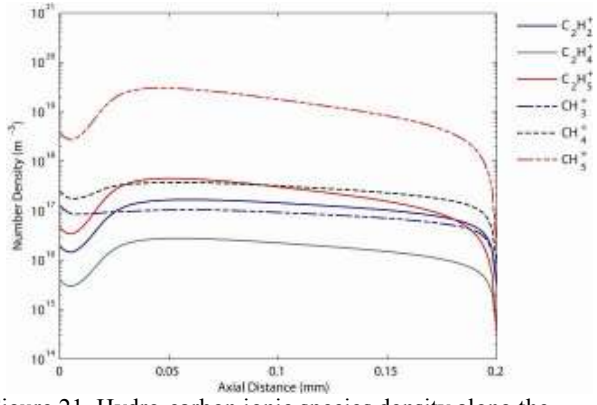

Figure 21. Hydro-carbon ionic species density along the axial distance (ballast resistance 200 kΩ, V_d = 248.76 V, I_d = 4.74 mA).

Of the different hydro-carbon ions, CH_5^+ was found to be the dominant ion (Figure 21). However comparing to the H_3^+ ions, CH_5^+ ions were found to be smaller by a factor of 3. The CH_5^+ number density distribution indicate volumetric production of CH_5^+ in the discharge, with the peak being in between the cathode sheath and the bulk plasma volume. The second dominant hydro-carbon ion was $C_2H_5^+$ which had a peak value of 4 x 10^{17} m^{-3}. The number density profile of $C_2H_5^+$ was similar to that of CH_5^+. Being three orders of magnitude smaller than CH_5^+ the $C_2H_4^+$ ion was found to be the least dominant.

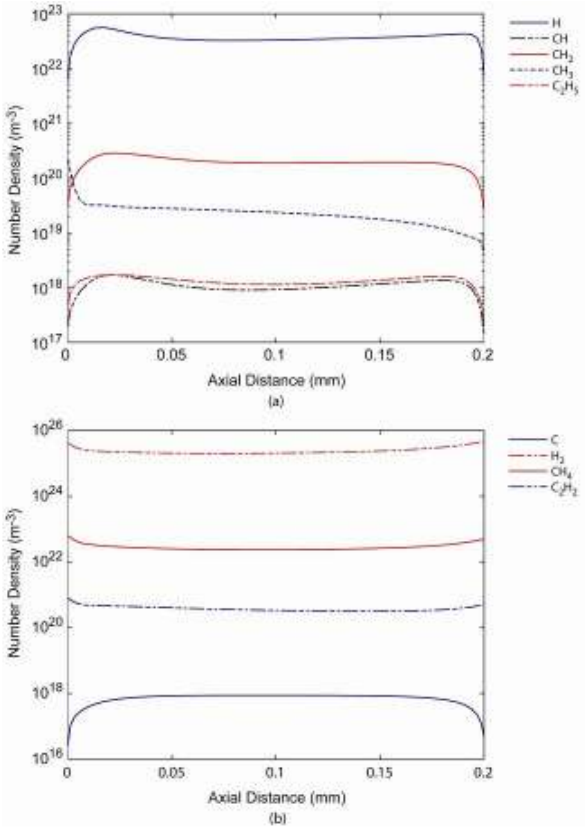

Figure 22. a) Radical species density and b) neutral species density along the axial distance (ballast resistance 200 kΩ, V_d = 251.1 V, I_d = 4.74 mA).

The distribution of the different radicals and neutrals along the axial distance are shown in Figure 22. Atomic H was found to be the dominant radical. A peak H density of 6 x 10^{22} m^{-3} was observed near the cathode, resulting in a dissociation degree of 0.002. The radical density distribution indicates the abundance of CH_2 and CH_3, CH_2 and CH_3 being dominant in the volume and in the sheath respectively. The peak densities of both these radicals were found to be in the order of 10^{21} m^{-3}. Both CH_2 and CH_3 are key components for DLC deposition [23]. The neutral density profiles show (Figure 22 (b)) C_2H_2 to be in the order of 10^{21} m^{-3} throughout the discharge. C_2H_2 was identified to be one of the key components for DLC deposition by other researchers [28, 29].

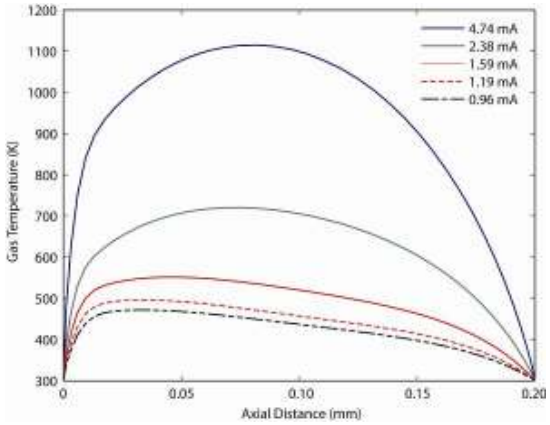

Figure 23. Gas temperature along the axial distance for different discharge current.

The neutral gas temperature profiles for different discharge currents are summarized in Figure 23. It can be seen that with an increase in the discharge current there is a rise in the neutral gas temperature. Increase in the discharge current results in an increase in the ion current density at the cathode. Ion joule heating being the key gas heating mechanism in atmospheric pressure micro-discharges [16, 30], the resulting larger ion current density increases the neutral gas temperature significantly. With an increase in the discharge current from 0.96 mA to 4.74 mA, the peak neutral gas temperature increased from 480 K to 1100 K. The peak neutral gas temperature was found to exist at the location of the peak ion densities.

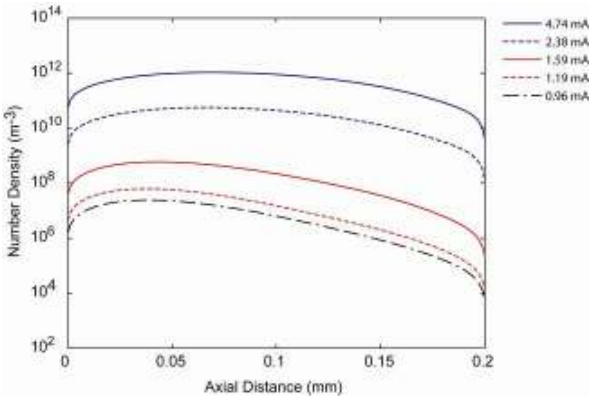

Figure 24. Soot number density along the axial distance for different discharge current.

The gas phase chemistry used in the model took into account the formation of soot from C_2H_2. The reaction rate constant for the soot formation reaction [$C_2H_2 \rightarrow$ Soot + H_2, $k_{soot} = 1.7 \exp(-7548/T_{gas})$] was taken from the literature [31]. Soot concentration profiles for different discharge current are shown in Figure 24. It is observed that with an increase in the gas temperature, the peak soot concentration increases from 10^6 to 10^{12} m^{-3}. A six order of magnitude increase is observed for ~ 600 K increase in the gas temperature. This suggests that the discharge would be more "Sooty" at higher power. To avoid the soot regime the micro-discharge needs to be operated at lower power.

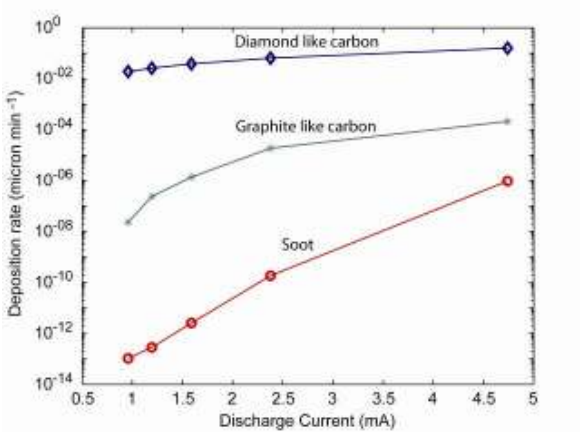

Figure 25. Deposition rates as a function of discharge of current.

Figure 25 shows the predicted deposition rates of DLC, graphitic carbon and soot for different discharge currents at the cathode surface. For lower discharge current the deposited film is more diamond like. In that regime the graphitic and the soot deposition rates are 6 and 11 orders of magnitude lower than the diamond like carbon. Even though the diamond-like and graphitic carbon deposition rates do not increase significantly, the soot deposition rate increases drastically with an increase in the discharge current. In the discharge current range of 0.96 – 4.74 mA, the soot deposition rate increases from 10^{-13} microns per minute to 10^{-7} microns per minute, an increase of 6 orders of magnitude. The deposition rate dependence on discharge current indicates a small window of operation for obtaining pristine diamond-like carbon thin film deposition.

3. SUMMARY OF WORK COMPLETED

Atmospheric pressure micro-plasmas have successfully been generated in our laboratory. The discharge was studied extensively both experimentally and numerically. The major findings from the studies are as follows:

Experimental

- Performed fundamental studies of the discharge characteristics of atmospheric pressure microplasmas.
- Determination of the relationships between gas composition, energy transfer, and gas temperature measurements for discharge in various atomic and molecular gases including hydrogen, helium, argon, air, nitrogen, and methane.
- Identification of instabilities as the major source of deposition roughness in AP-PECVD.
- Suppression of the ionization overheating instability using the external circuit in DC plasmas.
- Identification of excessive gas temperature and precursor concentration as the major controlling factors for particle formation. Particle formation was

identified as a secondary source of deposition roughness.

- Control of the discharge gas temperature using Helium gas mixtures.
- Deposition of uniform 'thin' film using stabilized and temperature reduced microplasmas.
- Studies of the parameter space and operating ranges corresponding to transition from 'thin' film to particle deposition.

Computational

- A hybrid model has been developed to provide insight into the physico-chemical properties of the discharge.
- Simulations were carried out for a hydrogen and a methane-hydrogen discharge powered by a DC power source.
- Numerical and experimental characterization of discharge in hydrogen compare favorably. Comparable features were: 1) normal current density, 2) negative glow and cathode sheath formation and 3) flat voltage current characteristics.
- It is found that heavier ions (H_3+ and H_2^+) are more dominant than the lighter ion (H^+) in hydrogen plasma at atmospheric pressure.
- The gas temperature prediction further indicates the discharge to be a non-thermal non-equilibrium discharge.
- For a methane-hydrogen the model predicted H_3^+ and CH_5^+ to be the dominant ionic species.
- CH_2, CH_3 and C_2H_2 were predicted to be the prominent radicals and neutrals which are the key components for DLC deposition.
- The gas temperature had significant affect on soot formation and deposition.
- The model predicted the discharge power to be the key factor to obtain pristine DLC deposition. Even though high power is desirable to increase the deposition rate, it significantly increases the soot deposition rate and hampers the film quality.

Our findings enable us to conclude that the atmospheric microdischarge can successfully be used for deposition purposes. The plasma is shown to be non-thermal in nature and thus highly selective and efficient in stimulation of chemical reactions. Localized reactions can be carried out with the microdischarge for depositing metals, insulating materials and polymers under atmospheric pressure condition, i.e. without the need for high vacuum.

Acknowledgements

The research reported is supported by the US National Science Foundation under grant # DMI-0423409.

REFERENCES

[1] D. Staack, B. Farouk, A. Gutsol, and A. Fridman, "Spectroscopic studies and rotational and vibrational temperature measurements of atmospheric pressure normal glow plasma discharges in air," *Plasma Sources Science and Technology,* vol. 15, pp. 818-827, 20 September 2006.

[2] Y. P. Raizer, *Gas Discharge Physics* . Berlin: Springer, 1997.

[3] D. Staack, B. Farouk, A. Gutsol, and A. Fridman, "Characterization of a dc atmospheric pressure normal glow discharge," *Plasma Sources Science and Technology,* vol. 14, pp. 700-711, 2005.

[4] C. Laux, "Radiative and Non-Equilibrium collisional-radiative models," in *von Karman Institute Special Course on Physico-chemical Modeling of High Enthalpy and Plasma Flows*, Rhose-Saint-Genesem Belgium, 2002.

[5] A. Fridman and L. Kennedy, *Plasma Physics and Engineering*. New York: Taylor and Francis 2004.

[6] B. Shokri and A. R. Niknam, "Discharge plasma instabilities in the presence of an external constant electric field," *Physics of Plasmas,* vol. 10, pp. 4153-4161, October 2003.

[7] A. A. Barmin, A. P. Glinoc, and G. A. Shoumova, "Overheating instability of an electric discharge stabilized by nonisothermal walls," *High Temperature (Teplofizika Vysokikh Temperatur),* vol. 25, pp. 626-632, Mar. 1988.

[8] T. Cserfalvi, P. Mezei, and P. Apai, "Emission studies on a glow discharge in atmospheric pressure air using water as a cathode," *Journal of Physics D: Applied Physics,* vol. 26, pp. 2184 - 2188, 1993.

[9] T. Cserfalvi and P. Mezei, "Operating mechanism of the electrolyte cathode atmospheric glow discharge," *Fresenius' Journal of Analytical Chemistry,* vol. 355, pp. 813 - 819, 1996.

[10] P. Mezei, T. Cserfalvi, and M. Janossy, "The gas temperature in the cathode surface-dark space boundary layer of an electrolyte cathode atmospheric glow discharge (ELCAD)," *Journal of Physics D: Applied Physics,* vol. 31, pp. L41 - L42, 1998.

[11] H. Kawamoto and S. Umezo, "Electrohydrodynamic deformation of water surface in a metal pin to water plate corona discharge system," *Journal of Physics D: Applied Physics,* vol. 38, 2005.

[12] P. Andre, Y. Barinov, G. Faure, V. Kaplan, A. Lefort, S. Shkol'nik, and D. Vacher, "Experimental study of discharge with liquid non-metallic (tap water) electrodes in air at atmospheric pressure," *Journal of Physics D: Applied Physics,* vol. 34, pp. 3456 - 3465, 2001.

[13] Y. Akishev, M. Grushin, I. Kochetov, V. Karal'nik, A. Napartovich, and N. Trushkin, "Negative corona, glow and spark discharges in ambient air and transitions between them," *Plasma Source Science and Technology,* vol. 14, pp. S18-S25, May 2005.

[14] D. Staack, B. Farouk, A. Gutsol, and A. Fridman, "Characterization of a dc atmospheric pressure normal glow discharge," *Plasma Source Science and Technology,* vol. 14, pp. 700-711, Nov 2005.

[15] S. D. Rockwood, "Elastic and Inelastic Cross-Sections for Electron-Hg Scattering from Hg Transport Data," *Physical Review A,* vol. 8, pp. 2348-2358, 1973.

[16] T. Farouk, B. Farouk, D. Staack, A. Gutsol, and A. Fridman, "Simulation of dc atmospheric pressure argon micro-glow discharge," *Plasma Sources Science and Technology,* vol. 15, pp. 676-688, 2006.

[17] V. Kolobov, "Fokker-Planck modelling of electron kinetics in plasmas and semiconductors " *Computational Material Science,* vol. 28, pp. 302-320, 2003.

[18] C. Chen, T. Wei, L. R. Collins, and J. Phillips, "Modelling the discharge region of a microwave generated hydrogen plasma " *Journal of Physics D: Applied Physics,* vol. 32, pp. 688-698, 1998.

[19] K. Hassouni, A. Gicquel, M. Capitelli, and J. Loureiro, "Chemical kinetics and energy transfer in moderate pressure H2 plasmas used in diamond MPACVD processes," *Plasma Sources Science and Technology,* vol. 8, pp. 494-512, 1999.

[20] CFD Research Corporation, "CFD-ACE Module Manual," Huntsville: ESI US R&D Inc, 2003.
[21] B. Johnson, T. Quarles, A. Newton, D. Pederson, A. Sangiovanni -Vincentelli, and C. Wayne, "SPICE3 Version 3e User's Manual Department of Electrical Engineering and Computer Sciences " Berkeley: University of California Press, 1991.
[22] T. Farouk, B. Farouk, D. Staack, A. Gutsol, and A. Fridman, "Modeling of direct current micro-plasma discharges in atmospheric pressure hydrogen," *Plasma Sources Science and Technology,* vol. 16, pp. 619-634, 2007.
[23] Z. Huang, Z. Pan, Y. Wang, and A. Du, "Deposition of hydrocarbon molecules on diamond surfaces (001) surfaces: atomic scale modeling," *Surface and Coatings Technology,* vol. 158-159, pp. 94-98, 2002.
[24] E. Dekempeneer, J. Smeets, L. Meneve, L. Eersels, and R. Jacobs, *Thin Solid Films,* vol. 241, p. 269, 1994.
[25] A. Gicquel, E. Anger, M. Ravet, D. Fabre, and G. Scatena, "Diamond deposition in a bell-jar reactor: influence of the plasma and substrate parameters on the microstructure and growth rate," *Diamond and Related Material,* vol. 2, pp. 417-424, 1993.
[26] K. Tachibana, M. Nishida, H. Harima, and Y. Urano, "Diagnostics and modelling of a methane plasma used in the chemical vapor deposition of amorphous carbon films " *Journal of Physics D: Applied Physics,* vol. 17, pp. 1727-1742, 1984.
[27] V. Ivanov, O. Proshina, T. Rakhimova, and A. Rakhimov, "Comparison of a one-dimensional particle in cell Monte-Carlo model and a one dimensional fluid model for a CH4/H2 capacitively coupled radio frequency discharge," *Journal of Applied Physics,* vol. 91, pp. 6298-6302, 2002.
[28] M. Coltrin and D. Dandy, "Analysis of diamond growth in subatmospheric dc plasma-gun reactors," *Journal of Applied Physics,* vol. 74, pp. 5803-5820, 1993.
[29] E. Neyts, A. Bogaerts, R. Gijbels, J. Benedikt, and M. C. M. van de Sanden, "Molecular dynamics simulations for the growth of diamond-like carbon films from low kinetic energy species," *Diamond and Related Material,* vol. 13, pp. 1873-1881, 2004.
[30] Q. Wang, D. Economou, and V. Donnelly, "Simulation of a direct current microplasma discharge in helium at atmospheric pressure," *Journal of Applied Physics,* vol. 100, pp. 023301-10, 2006.
[31] F. Liu, H. Guo, G. Smallwood, and O. Gulder, "Numerical modeling of soot formation and oxidation in laminar coflow non-smoking and smoking ethylene diffusion flames," *Combustion Theory and Modelling,* vol. 7, pp. 301-315, 2003.